molecular pharmaceutics

Article

pubs.acs.org/molecularpharmaceutics

^{64}Cu-Labeled Gp2 Domain for PET Imaging of Epidermal Growth Factor Receptor

Max A. Kruziki,[†] Brett A. Case,[†] Jie Y. Chan,[‡] Elizabeth J. Zudock,[†] Daniel R. Woldring,[†] Douglas Yee,[‡,§,∥] and Benjamin J. Hackel*[,†]

[†]Department of Chemical Engineering and Materials Science, [‡]Department of Pharmacology, [§]Department of Medicine, and [∥]Masonic Cancer Center, University of Minnesota−Twin Cities, 421 16th Avenue SE, Minneapolis, Minnesota 55455, United States

Supporting Information

ABSTRACT: This purpose of this study is to determine the efficacy of a 45-amino acid Gp2 domain, engineered to bind to epidermal growth factor receptor (EGFR), as a positron emission tomography (PET) probe of EGFR in a xenograft mouse model. The EGFR-targeted Gp2 (Gp2-EGFR) and a nonbinding control were site-specifically labeled with 1,4,7,10-tetraazacyclododecane-1,4,7,10-tetraacetic acid (DOTA) chelator. Binding affinity was tested toward human EGFR and mouse EGFR. Biological activity on downstream EGFR signaling was examined in cell culture. DOTA-Gp2 molecules were labeled with ^{64}Cu and intravenously injected (0.6−2.3 MBq) into mice bearing EGFR^{high} (n = 7) and EGFR^{low} (n = 4) xenografted tumors. PET/computed tomography (CT) images were acquired at 45 min, 2 h, and 24 h. Dynamic PET (25 min) was also acquired. Tomography results were verified with gamma counting of resected tissues. Two-tailed t tests with unequal variances provided statistical comparison. DOTA-Gp2-EGFR bound strongly to human (K_D = 7 ± 5 nM) and murine (K_D = 29 ± 6 nM) EGFR, and nontargeted Gp2 had no detectable binding. Gp2-EGFR did not agonize EGFR nor antagonize EGF-EGFR. ^{64}Cu-Gp2-EGFR tracer effectively localized to EGFR^{high} tumors at 45 min (3.2 ± 0.5%ID/g). High specificity was observed with significantly lower uptake in EGFR^{low} tumors (0.9 ± 0.3%ID/g, p < 0.001), high tumor-to-background ratios (11 ± 6 tumor/muscle, p < 0.001). Nontargeted Gp2 tracer had low uptake in EGFR^{high} tumors (0.5 ± 0.3%ID/g, p < 0.001). Similar data was observed at 2 h, and tumor signal was retained at 24 h (2.9 ± 0.3%ID/g). An engineered Gp2 PET imaging probe exhibited low background and target-specific EGFR^{high} tumor uptake at 45 min, with tumor signal retained at 24 h postinjection, and compared favorably with published EGFR PET probes for alternative protein scaffolds. These beneficial *in vivo* characteristics, combined with thermal stability, efficient evolution, and small size of the Gp2 domain validate its use as a future class of molecular imaging agents.

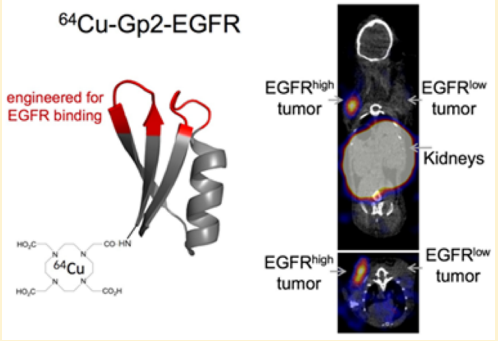

KEYWORDS: *Gp2 domain protein scaffold, epidermal growth factor receptor imaging, micropositron emission tomography, murine model*

INTRODUCTION

Molecular cancer therapeutics have provided effective treatments for many cancers, yet are typically characterized by efficacy on only a subset of patients, even within a type of cancer as defined by tissue.[1,2] Personalized or precision medicine via molecular characterization to differentiate responders from nonresponders can aid patient outcomes.[3] Epidermal growth factor receptor (EGFR) overexpression is present in many cancer types,[4−10] correlates with differentiation, reduced disease-free and overall survival, and is an independent prognostic indicator of poor survival in colorectal cancer patients.[11,12] EGFR amplification is predictive of response to cetuximab in wild-type KRAS metastatic colorectal cancer patients.[13−15] In HER2-positive primary breast cancer, EGFR overexpression, but not copy number, is a poor prognostic factor and predictive of response to trastuzumab.[16] The current biopsy/immunohistochemistry approach to EGFR characterization is invasive and does not account for spatiotemporal heterogeneity, most notably differential expression between primary tumors and metastases.[17−19] Positron emission tomography (PET) targeting EGFR could inform personalized treatment plans by enabling identification, localization, and characterization of primary tumors and metastases, while being noninvasive, quantitative, and sensitive to picomolar quantities. PET-based imaging has been clinically useful for other receptors, such as imaging estrogen receptor for breast cancer.[20,21]

Numerous scaffolds have been explored as molecular PET tracers of EGFR. Therapeutic monoclonal antibodies (∼150 kDa) have been radiolabeled to visualize EGFR in vivo but slow clearance results in high background and liver signal and

Received: June 15, 2016
Revised: September 28, 2016
Accepted: October 3, 2016
Published: October 3, 2016

DOI: 10.1021/acs.molpharmaceut.6b00538
Mol. Pharmaceutics 2016, 13, 3747−3755

necessitates late imaging times that elevate patient dose.[22−27] 94-Residue fibronectin domains,[28,29] 58-residue affibodies,[30−34] 120-residue nanobodies,[35−37] and 400-residue Fab fragments[38] have provided good tumor-to-background ratios at early time points (≤4 h) via nuclear imaging due to their fast clearance, better extravasation, and increased tissue penetration compared to antibodies.[39−42] Additional scaffolds have been used for other targets.[43] Small molecule inhibitors[44−49] and natural EGF ligand[50] provide molecular characterization but are not biologically passive.

We recently developed the 45-residue Gp2 domain as a small, stable protein scaffold that has been successfully evolved toward multiple targets with high affinity (0.2−18 nM K_d) while retaining thermal stability (65−80 °C).[51] The Gp2 scaffold contains a framework of a single α helix and three beta-strands, and two solvent-exposed loops that form the diversified paratope. Thermal stability, lack of cysteine, and presence of a single lysine residue distant from the proposed paratope provide ease of chemical conjugation of imaging moieties through amine or thiol chemistry. Additionally, the small size and straightforward structure enable direct chemical synthesis. The two Gp2 variants used here are Gp2-EGFR$_{2.2.3}$, which was previously evolved to bind to EGFR with 18 ± 8 nM affinity, and EGFR nonbinding control, Gp2-rIgG$_{3.2.3}$, which previously evolved to bind to an irrelevant control (rabbit IgG; notably the molecule does not cross-react with murine IgG) (herein referred to as Gp2-EGFR and Gp2-nb). These variants share 70% sequence identity (Table S1).

We hypothesize that the small size of Gp2 will provide high tumor uptake with fast blood clearance enabling high contrast images at early time points. The ease of evolution and synthesis combined with high thermal stability and different paratope topology may provide a useful tool as an alternative imaging agent to available molecules. In particular, variant Gp2-EGFR has 18 ± 8 nM affinity for cell-surface EGFR with a midpoint of thermal denaturation of 71 °C. The current study evaluates the ability of this scaffold to function as molecular PET agent in a small animal model.

EXPERIMENTAL SECTION

Protein Production and DOTA Conjugation. Gp2 domains were produced recombinantly in *E. coli* as described previously.[51] Briefly, one liter of LB medium with 50 mg/L kanamycin was inoculated with 5 mL of overnight BL21(DE3) *E. coli* culture carrying the pET-Gp2-His$_6$ plasmid, grown at 37 °C to an optical density (600 nm) of 0.6−1.5 units, and induced with 0.5 mM isopropyl β-D-1-thiogalactopyranoside for 20−24 h at 30 °C. Cells were pelleted, resuspended in 10 mL of lysis buffer (50 mM sodium phosphate (pH 8.0), 0.5 M NaCl, 5% glycerol, 5 mM 3-[(3-cholamidopropyl) dimethylammonio]-1-propanesulfonate, and 25 mM imidazole), and underwent four freeze−thaw cycles. The soluble fraction was isolated by centrifugation at 12,000*g* for 10 min. Gp2 was purified by metal affinity chromatography on a HisPur resin (Pierce, Thermo Fisher Scientific). Purified Gp2, 30−60 μM, in PBS containing 150 mM imidazole was mixed with 25- to 50-fold molar excess 10 mg/mL DOTA-NHS-ester (Macrocyclics) in dimethyl sulfoxide and allowed to react at room temperature for 1 h. The reaction was quenched with excess 1 M Tris pH 8.0, purified on a PD-10 column (GE Healthcare), and evaluated by matrix-assisted laser desorption ionization mass spectrometry.

Size Exclusion Chromatography. Protein solutions in 100 mM sodium acetate at pH 5.0 were filtered with a 0.2 μM filter to remove any particulates. Two hundred microliters of 40 μM DOTA-Gp2 was loaded onto an AKTA primeplus (GE Healthcare Bio-Sciences) and with a Superdex 75 10/300 GL column. The mobile phase was 100 mM sodium acetate at pH 5.0 flowing at 0.5 mL/min.

Cell Growth. A431 epidermoid carcinoma were kindly provided by Dr. Daniel Vallera (University of Minnesota). MDA-MB-435 cells, which have similarities to a melanoma cell line but also show evidence of breast cancer lineage,[52] were kindly provided by Dr. Tim Starr (University of Minnesota). Cells were cultured in Dulbecco's modified Eagle's medium with 10% fetal bovine serum at 37 °C in humidified air with 5% CO_2.

Affinity Measurement. Cells to be used in flow cytometry were detached using trypsin for a shorter time (3−5 min) than recommended. Detached cells were washed and labeled with Gp2 at varying concentrations for 15−30 min at 4 °C. Cells were pelleted and washed with PBSA (PBS + 0.1% w/v BSA), then labeled with fluorescein-conjugated rabbit anti-His$_6$ antibody (Abcam ab1206) for 15 min at 4 °C. Fluorescence was analyzed on a C6 Accuri flow cytometer (BD Biosciences). The equilibrium dissociation constant, K_D, was identified by minimizing the sum of squared errors assuming a 1:1 binding interaction.

Affinity of Gp2 toward soluble murine EGFR ectodomain (Sino Biological) was determined using Gp2 displayed on the yeast surface as described previously.[51]

Western Blot Analysis. A431 cells were grown to approximately 60% confluency, washed with PBS, and incubated in serum-free medium overnight at 37 °C in humidified air with 5% CO_2. The next day, cells were washed with PBS and exposed to four different conditions at 37 °C: (1) PBS for 20 min; (2) 5 nM DOTA-Gp2-EGFR for 20 min; (3) 5 nM epidermal growth factor (Gemini Bio Products) for 20 min; or (4) 5 nM DOTA-Gp2-EGFR for 30 min, washed with PBS, followed by 5 nM epidermal growth factor for 20 min. Cells were detached from the plate by mechanical shearing in RIPA buffer (PBS with 1% v/v Triton X-100, 0.5% w/v sodium deoxycholate, 0.1% w/v sodium dodecyl sulfate). Cells were lysed through rotation at 4 °C for 30 min in RIPA buffer. After centrifuging at 15,000*g* for 15 min at 4 °C the supernatant was collected and protein concentration was determined with a Pierce BCA assay kit (Thermo Scientific).

Whole-cell lysates (60 μg) were boiled in 5× Laemmli loading buffer at 95 °C for 5 min, separated by 8% SDS-PAGE, transferred to PVDF membrane, and subjected to indicated immunoblotting analyses according to manufacturer guidelines. The primary antibodies bind phosphorylated AKT serine 473 (#9271 Cell Signaling Technology), total AKT (#9272), phosphorylated EGFR tyrosine 1068 (#2234), total EGFR (#2232S), and actin (#A3853 Sigma-Aldrich) were incubated overnight at 4 °C. After washing with Tris-buffered saline with Tween-20 (50 mM Tris, 150 mM sodium chloride, and 0.05% Tween-20), the membrane was further immunoblotted with either antirabbit horseradish peroxidase-conjugated antibody (#NA934 V GE Healthcare Life Science) or antimouse horseradish peroxidase-conjugated (#170-6516 Biorad) secondary antibody for 1 h at 37 °C.

Internalization. Gp2-EGFR and Gp2-nb in PBS with 150 mM imidazole was allowed to react with fluorescein isothiocyanate in DMSO (3 mg/mL) at 100× molar excess at

DOI: 10.1021/acs.molpharmaceut.6b00538
Mol. Pharmaceutics 2016, 13, 3747−3755

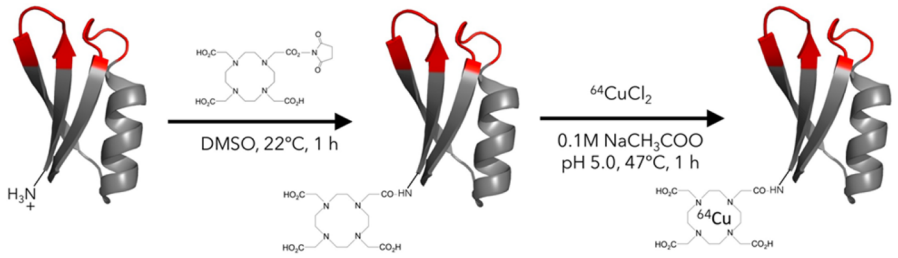

Figure 1. Gp2 conjugation. Purified Gp2 was conjugated with the *N*-hydroxysuccinimidyl ester of the chelator DOTA then radiolabeled with ^{64}Cu.

room temperature for 1 h. The reaction was quenched with excess 1 M Tris buffer pH 8, purified on a Zeba Spin Desalting Column 7K molecular weight cutoff (ThermoFisher). Fluorescein conjugation was verified by matrix-assisted laser desorption ionization mass spectrometry.

A431 and MDA-MB-435 cells were grown and detached as above. Cells were labeled with 100 nM fluorescein conjugated Gp2 at 37 °C for 0.5 and 1 h, followed by incubation with 0.2 M acetic acid, 0.5 M NaCl pH 2 for 5 min to strip extracellular binding. Fluorescence was detected by flow cytometry. Internalization was calculated by normalizing the change in fluorescence signal over time to fluorescence signal of A431 cells labeled with 100 nM fluorescein-Gp2-EGFR at 4 °C for 0.5 h.

Copper Chelation and Purification. $^{64}CuCl_2$ (UW-Madison) was diluted into 150 μL of 100 mM sodium acetate pH 5.0 and pH adjusted to pH 5.0. Approximately 50 MBq of the $^{64}CuCl_2$ was added to 100 μL of DOTA-Gp2 in 100 mM sodium acetate pH 5.0 at 30−60 μM. The mixture was allowed to incubate at 47 °C for 1 h and purified by PD-10 column equilibrated with 10 mM sodium acetate pH 5.0 in order to remove unchelated copper.

Radio TLC. One microliter of ^{64}Cu-Gp2 was spotted on filter paper, and a mobile phase of PBS was applied for 20 min. An AR-2000 radio-thin layer chromatography scanner (Eckert and Ziegler) scanned and analyzed the filter paper for migration of radioactive peaks. Comparison of scans before and after PD-10 purification showed removal of the peak near the solvent front (the unconjugated ^{64}Cu) while retaining the less mobile peak (^{64}Cu-Gp2), which cold PD-10 purifications along with SDS-PAGE and binding assays have shown to contain highly pure Gp2.

Tumor Inoculation. Eight week old female (*Foxn1^{nu}*/*Foxn1^{nu}*) mice (Jackson Laboratory) were anesthetized with 1.5% isoflurane in 1 mL/min O_2 and subcutaneously injected with 10 million MDA-MB-435 cells in 50% v/v Matrigel Matrix (Corning) in one shoulder. After 4 weeks, the mice were injected with two million A431 cells in 50% Matrigel Matrix into the opposite shoulder. Xenografted tumors were grown to 5−10 mm in diameter (approximately 2 weeks for A431 and 6 weeks for MDA-MB-435).

EGFR Expression Quantification. To quantify EGFR expression within *in vivo* xenografted tumor cells, GentleMACS dissociator C Tubes (Miltenyi Biotec) were used to generate single cell suspensions from excised tumors. Receptor expression was quantified by flow cytometry with Quantum Simply Cellular antimouse IgG calibration beads (Bang's Laboratories), using Gp2-EGFR and/or mouse anti-EGFR antibody (Abcam ab30) at 1 μM, followed by secondary labeling with fluorescein conjugated rabbit anti-His6 (Abcam ab1206) or AlexaFluor 647 conjugated goat antimouse IgG (ThermoFisher), respectively. The cell population from the A431 tumor was approximated as two normally distributed subpopulations.

PET Imaging: Static and Dynamic. All procedures performed in studies involving animals were in accordance with the ethical standards of the University of Minnesota and approved by the Institutional Animal Care and Use Committee. Mice were anesthetized with 1.5% isoflurane in 1 mL/min O_2 and tail vein injected with approximately 0.6 to 2.3 MBq of ^{64}Cu-Gp2 as measured by a Atomlab 100 dosimeter with a setting of 50.2. Five-minute static PET scans were performed at 45 min, 2 h, and 24 h after injection using an Inveon micro-PET/CT (Siemens). The PET energy cutoffs were 350−650 keV with a timing window of 3.438 ns. The PET images were reconstructed with an OSEM2D method using four iterations of Fourier rebinning. PET images were smoothed with a 1 × 1 × 1 voxel Guassian filter. The CT used 340 projections of 80 kV at 500 μA with 200 ms exposure over 384 s of total scan time with an effective pixel size of 98.3 μm. The CT was reconstructed using the Feldkamp algorithm with a Shepp-Logan filter. The preceding methods are included in the Inveon Acquisition Workplace software (Siemens). A second batch of independently produced, DOTA-conjugated, ^{64}Cu chelated, and purified ^{64}Cu-Gp2-EGFR injected into another set of tumor inoculated mice validated the results of the other 45 min and 2 h PET/CT scans.

PET images were quantified using the Inveon Research Workplace software (Siemens). Using the CT as an anatomical guide, the volume of 10−20 mm^3 that resulted in the maximum average PET signal for that tissue was selected. The anterior end of the liver was selected to avoid noise from kidney signal. The posterior leg furthest from any bladder signal was chosen to represent muscle background.

Tissue Gamma Counting. After imaging, mice were euthanized by cervical dislocation under isoflurane anesthesia. Blood, bone, brain, heart, large intestine, kidneys, liver, lungs, muscle, pancreas, skin, spleen, stomach, and tumors were resected, weighed, and had their activity measured by a CRC-25W (Capintec) gamma counter averaged over 45 s. The CRC-25W collected counts from all windows and was calibrated through serial dilutions based on the dose reported by the Atomlab 100 dosimeter used to measure injected dose. Renal radiation dose was calculated with the Medical Internal Radiation dose method.

Statistics. Comparisons between two samples were determined using a two-tailed student's *t* test for unequal variances. P-values are stated where relevant. Data are presented as average ± standard deviation.

DOI: 10.1021/acs.molpharmaceut.6b00538
Mol. Pharmaceutics 2016, 13, 3747−3755

RESULTS

Gp2 Production and Conjugation. EGFR-binding Gp2-EGFR and nonbinding control Gp2-nb, both containing a C-terminal His-6 tag, were produced in the soluble fraction of *E. coli* and purified by immobilized metal affinity chromatography. Purity was verified with SDS-PAGE, and molecular weight was verified by matrix assisted laser desorption ionization mass spectrometry (Gp2-EGFR expected, 6873; actual, 6869. Gp2-nb expected, 6228; actual, 6226). The copper chelator 1,4,7,10-tetraazacyclododecane-1,4,7,10-tetraacetic acid (DOTA) was conjugated to the N-terminal lysine residue distal from the proposed paratope in the Gp2 scaffold framework (Figure 1). Mass spectrometry was used to verify an average labeling of 0.83 DOTA per molecule for Gp2-EGFR and 1.1 DOTA per molecule for Gp2-nb (Figure S1). Size exclusion chromatography verified that DOTA-Gp2-EGFR (7.4 kDa) is dominantly monomeric, eluting at a comparable time to control proteins of a similar size (6.5 kDa aprotinin and 7.5 kDa affibody; Figure S2).

EGFR Binding. Gp2-EGFR binding affinity toward cellular EGFR was previously found to be 18 ± 8 nM.[51] The effect of DOTA conjugation on binding affinity was examined by labeling EGFR-expressing A431 epidermoid carcinoma cells with varying levels of DOTA-Gp2-EGFR. DOTA conjugation did not significantly change ligand affinity (7 ± 5 nM; Figure 2). The nonbinding control DOTA-Gp2-nb showed no detectable binding up to 300 nM on A431 cells (Figure 2). Preclinical imaging experiments with EGFR targeted Gp2 were carried out in mice, so the affinity of Gp2-EGFR toward murine EGFR was examined. Yeast displaying Gp2-EGFR were labeled with varying levels of recombinantly produced murine EGFR extracellular domain, which revealed an affinity of 29 ± 6 nM (Figure S3).

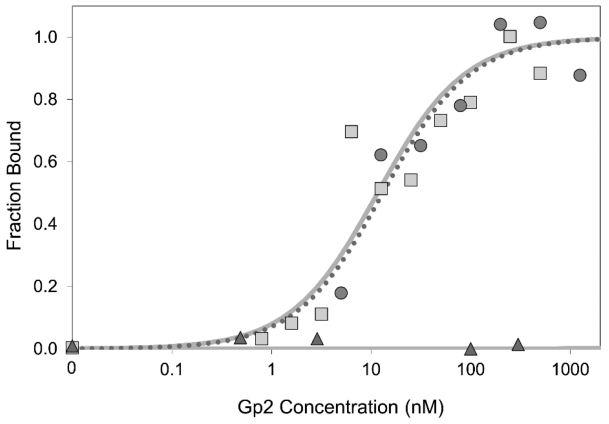

Figure 2. Affinity titration. A431 cells were labeled with DOTA-Gp2 domains (squares, DOTA-Gp2-EGFR; triangles, DOTA-Gp2-nb) at the indicated concentrations. Binding was detected by fluorescein-conjugated anti-His_6 antibody via flow cytometry. Fluorescence signal is normalized between minimal and maximal fluorescence. One representative titration of triplicate experiments is presented. A representative Gp2-EGFR titration curve is also included for comparison (circles, dotted line). The equilibrium dissociation constant for DOTA-Gp2-EGFR, assuming a 1:1 binding model, is 7 ± 5 nM.

Biological Activity. The effect of DOTA-Gp2-EGFR binding on the EGFR signaling pathway was determined by Western blot to detect phosphorylated AKT (p-AKT at S473), a downstream protein kinase, and phosphorylated EGFR (p-EGFR at Y1068) (Figure 3a). A431 cells labeled with 5 nM DOTA-Gp2-EGFR show no change in p-AKT or p-EGFR compared to PBS only control suggesting that DOTA-Gp2-EGFR is not agonistic to EGFR, DOTA-Gp2-EGFR is also not antagonistic, as blocking the A431 cells with 5 nM Gp2 before addition of 5 nM epidermal growth factor showed no change in level of p-AKT or p-EGFR compared to EGF only control.

The ability of A431 cells to internalize Gp2 was examined through flow cytometry of cells grown in tissue plate culture. Fluorescein was conjugated to Gp2-EGFR (0.45 fluorescein/protein) and Gp2-nb (0.61 fluorescein/protein) through amine chemistry and used to label A431 and MDA-MB-435 cells at 37 °C for up to 1 h. At 0.5 and 1 h, cells were acid stripped, and the increase in signal over time was used to calculate internalization rate (Figure 3b). Fluorescein-Gp2-EGFR rapidly internalized into A431 cells (2.2 ± 0.3-fold of saturated surface EGFR per hour) compared to control cells (MDA-MB-435, $p < 0.001$) and control nonbinder (fluorescein-Gp2-nb, $p < 0.001$).

Copper Chelation and Purification. Radioactive ^{64}Cu was incubated with DOTA-Gp2 for 1 h at 47 °C. Free ^{64}Cu was separated by size exclusion chromatography resulting in, on average, 93% purity. Labeling efficiency was 29%, perhaps due to the low number of DOTA per Gp2 (to ensure site specific conjugation) or modest protein concentration. Based on historical yields from nonradioactive DOTA-Gp2 purifications, the specific activity of chelated protein was 0.6−1.1 MBq/nmol. Radiolabeled DOTA-Gp2 variants are referred to as ^{64}Cu-Gp2-EGFR or ^{64}Cu-Gp2-nb.

Murine Model Micro-PET/CT and Tissue Biodistribution. The efficacy of the Gp2 domain was evaluated in a murine model with xenografted human tumor lines. To assess specificity $EGFR^{high}$ A431 tumors (mean, 5.2×10^5 EGFR/cell; 75th percentile, 1.9×10^6) and $EGFR^{low}$ MDA-MB-435 tumors (mean and 75th percentile, $<4 \times 10^3$ EGFR/cell) (Figure S4) were simultaneously evaluated. A nonbinding Gp2 domain was tested in parallel. ^{64}Cu-Gp2 was injected via the tail vein into mice harboring dual tumors. PET/CT was performed at 45 min and 2 h. ^{64}Cu-Gp2-EGFR effectively localized to A431 tumors highly expressing EGFR (3.2 ± 0.5%ID/g) and cleared from background (11 ± 6 tumor/background ratio, $p < 0.001$) as early as 45 min after injection (Figure 4). Targeting was molecularly specific as $EGFR^{low}$ MDA-MB-435 tumors had demonstrably lower signal (0.9 ± 0.3%ID/g, $p < 0.001$). Moreover, the nontargeted control ^{64}Cu-Gp2-nb exhibited lower signal in $EGFR^{high}$ tumors (0.5 ± 0.3%ID/g, $p < 0.001$). As for most small protein imaging agents, high kidney signal is observed (78 ± 16%ID/g) resulting from renal processing. Similar imaging is observed at 2 h where ^{64}Cu-Gp2-EGFR uptake to $EGFR^{high}$ tumors was 3.2 ± 0.6%ID/g and 12 ± 4 tumor/background ($p = 0.006$). Specificity is retained at 2 h as $EGFR^{low}$ tumors had low uptake (0.7 ± 0.2%ID/g, $p = 0.009$) and the nontargeted control had lower signal in $EGFR^{high}$ tumors (0.7 ± 0.3%ID/g, $p = 0.007$). While early time point imaging is the preferred translational route, we acknowledge that for alternative applications, such as targeted therapy, and biological safety concerns the behavior of engineered proteins at later times is relevant. Even with the fast clearance, preferential $EGFR^{high}$ tumor signal from ^{64}Cu-Gp2-EGFR is still evident at 24 h (2.9 ± 0.3%ID/g) with high tumor/background (8 ± 6, $p = 0.009$).

PET images were corroborated by ex vivo tissue gamma counting at 2 and 24 h (Figure 5). At 2 h postinjection, ^{64}Cu-

DOI: 10.1021/acs.molpharmaceut.6b00538
Mol. Pharmaceutics 2016, 13, 3747−3755

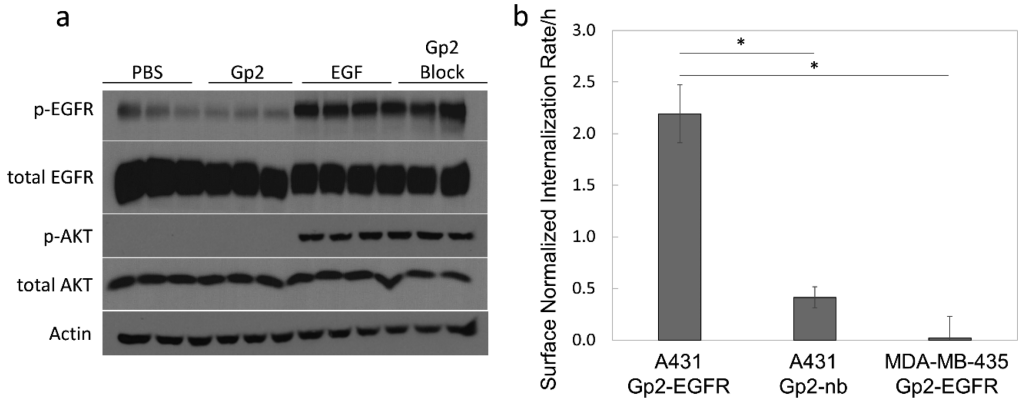

Figure 3. Biological activity. (a) A431 cells were labeled with four different conditions in triplicate: PBS only, 5 nM DOTA-Gp2-EGFR in PBS, 5 nM epidermal growth factor (EGF) in PBS, or 5 nM DOTA-Gp2-EGFR followed by 5 nM EGF (Gp2 block). Cells were lysed and separated by SDS-PAGE. Blotting was done to detect phosphorylated AKT (S473), a protein kinase in the EGFR signaling pathway, and phosphorylated EGFR (Y1068), as well as total amounts of the two proteins and actin to verify similar total protein concentration. DOTA-Gp2-EGFR is neither agonistic, since it does not activate the EGFR pathway, nor antagonistic, since it does not block activation when EGF is present. (b) A431 and MDA-MB-435 cells were labeled with 100 nM fluorescein conjugated Gp2 at 37 °C for 0.5 and 1 h, followed by incubation with acid for 5 min to strip extracellular binding. Internalization was calculated by normalizing the change in fluorescence signal over time to fluorescence signal of A431 cells labeled with 100 nM fluorescein-Gp2-EGFR at 4 °C for 0.5 h. Error bars represent standard deviation for $n = 3$ biological replicates. $P < 0.001$ is indicated by *.

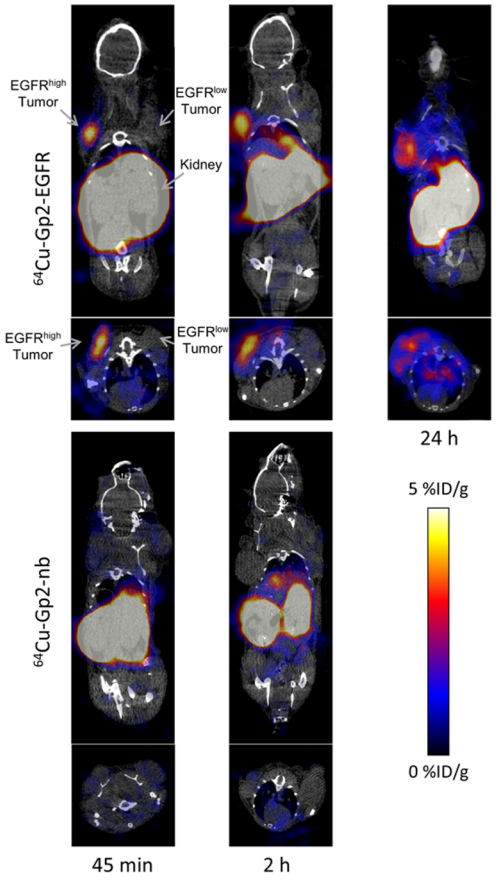

Figure 4. PET/CT imaging. Coronal and axial micro-PET/CT images of anesthetized athymic nude mice bearing subcutaneously xenografted A431 tumors ($EGFR^{high}$) in the left shoulder and MDA-MB-435 tumors ($EGFR^{low}$) in the right shoulder. The mouse in the 24 h image lacks a MDA-MB-435 tumor. Mice were injected by tail vein with 0.6–2.6 MBq of either ^{64}Cu-Gp2-EGFR (top row) or the nontargeted control, ^{64}Cu-Gp2-nb (bottom row). Five minute static PET scans followed by CT scans were acquired at 45 min (left), 2 h (middle), and 24 h (right, for targeted Gp2 only) postinjection. Image planes were selected such that both tumors appear in the image.

Gp2-EGFR localized significantly more to xenografted $EGFR^{high}$ tumors (7.0 ± 1.9% ID/g) as compared to $EGFR^{low}$ tumors (1.4 ± 0.3% ID/g; $p < 0.001$). The targeted Gp2 had 14 ± 8 tumor-to-blood ratio and 23 ± 6 tumor-to-muscle at 2 h, compared to 1.8 ± 1 tumor-to-blood ($p = 0.005$) and 3.3 ± 3.1 tumor-to-muscle ($p < 0.001$) for the nontargeted Gp2. In addition, the nontargeted Gp2 showed significantly lower $EGFR^{high}$ tumor uptake with 1.4 ± 0.4% ID/g ($p = 0.001$). Renal retention was high for the targeted (244 ± 66%ID/g) and nontargeted (208 ± 19%ID/g) probes. Liver signal was modest for both (4.8 ± 1.8 and 4.9 ± 1.9%ID/g). At 24 h the fast clearance leads to lower signal in most tissues, including $EGFR^{high}$ tumor (4.0 ± 0.3%ID/g) and kidney (114 ± 20%ID/g), with the exception of a notable increase in liver signal (10.1 ± 1.3%ID/g). Tumor-to-blood and tumor-to-muscle ratios (3.4 ± 1.1, $p = 0.002$ and 8.1 ± 3.6, $p < 0.001$, respectively) indicate there is still preferential uptake to $EGFR^{high}$ tumor.

The rapid distribution and clearance of ^{64}Cu-Gp2 evident at the 45 min scan was more thoroughly investigated by 25 min dynamic PET scans (Figure 6). Using heart signal as a surrogate for probe blood levels, clearance half-time was revealed to be 3.2 ± 1.0 min, supporting the low accumulation in muscle background seen at 45 min postinjection.

DISCUSSION

Other small scaffolds have been successfully used for in vivo imaging previously, but drawbacks, such as the relatively larger size of fibronectins (11 kDa)[53] and DARPins (20 kDa)[54] or the difficultly of broad evolution and presence of cysteines in knottins[55] and cyclic peptides,[56] have driven the search for additional scaffolds. Cysteine-free affibodies[57] have gone to smaller size (58 amino acids) and their helical paratope has yielded high affinity binders; however, they are typically severely destabilized after mutation.[58] Gp2 domains push the size even smaller (45–49 amino acids), have thus far remained highly thermally stable after mutation, and provide a vastly different paratope structure compared to affibodies. Beyond its previous characterization for high-affinity, EGFR-specific binding,[51] further biophysical evaluation of Gp2-EGFR in the current study revealed that it is well-suited for use in molecular

DOI: 10.1021/acs.molpharmaceut.6b00538
Mol. Pharmaceutics 2016, 13, 3747–3755

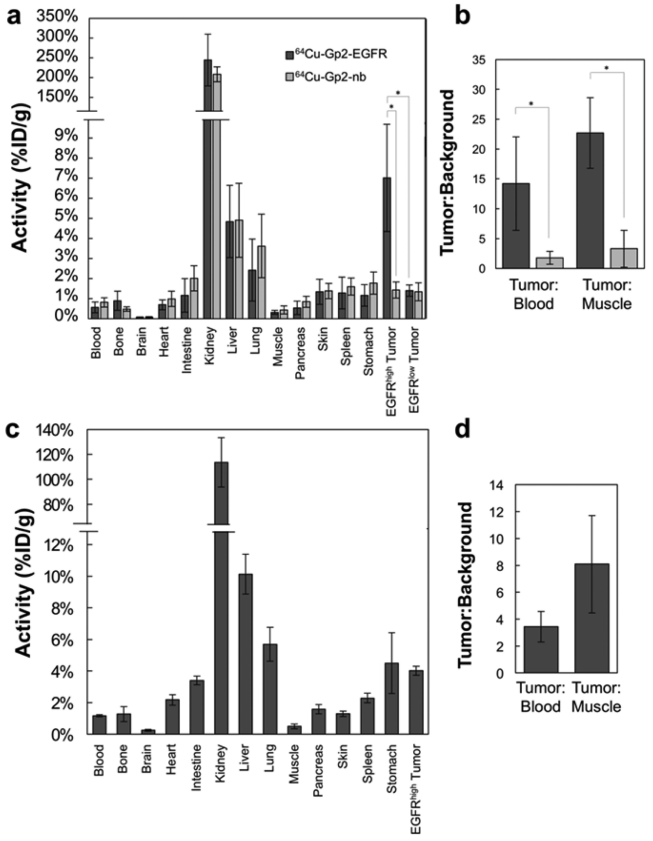

Figure 5. Resected tissue gamma counting. After PET/CT imaging, mice were euthanized and tissues were collected, weighed, and measured for activity. (A) The targeted ^{64}Cu-Gp2-EGFR (dark gray) and nontargeted ^{64}Cu-Gp2-nb (light gray) distribution is shown for the selected tissues at 2 h postinjection. (B) Ratios of tumor signal to relevant background signals in blood and muscle. The data is combined over two separate experiments, n = 4 for mice containing EGFR^{high} and EGFR^{low} tumors and another n = 3 for mice containing only EGFR^{high} tumors. Significance for important comparisons (p < 0.005) is denoted by *. (C,D) Biodistribution and tumor-to-background ratios of ^{64}Cu-Gp2-EGFR in n = 3 mice at 24 h postinjection. Error bars represent standard deviation.

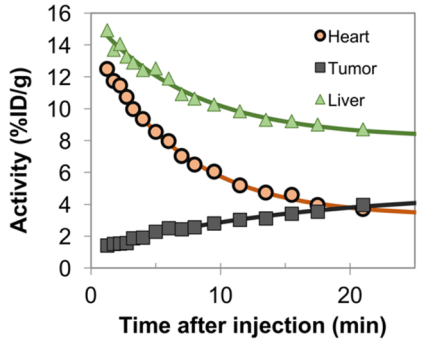

Figure 6. Dynamic PET scans. Twenty-five minute dynamic PET scans were acquired on anesthetized mice containing xenografted EGFR^{high} tumors. The average signal within ~15 mm^3 regions, guided by an anatomical CT scan, is presented. Data were fit assuming exponential kinetics. The clearance half-time within the heart (predominantly blood pool) was $t_{1/2}$ = 3.2 ± 1.0 min (n = 2 mice).

imaging. Though selected solely for EGFR ectodomain binding, the current Gp2 variant is neither agonistic nor antagonistic (Figure 3a). This enables passive imaging, unlike radiolabeled EGF or bivalent, cross-linking-compatible antibodies, which is preferred to avoid impacting EGF signaling cascades. Additionally, Gp2-EGFR is internalized into A431 cells (Figure 3b). Internalization potentially allows for an accumulation of signal in target tissues over time, but may not be highly relevant for Gp2 due to the rapid clearance of the small agent, which has the benefit of reducing background. Primary amine/*N*-hydroxysuccinimidyl chemistry was selected for conjugation at the N-terminal lysine distal to the evolved loops (Figure 1). As hoped, DOTA conjugation did not hinder binding affinity (18 ± 8 nM as Gp2-EGFR to 7 ± 5 nM as DOTA-Gp2-EGFR). Importantly, Gp2-EGFR exhibits cross-reactive binding to murine EGFR, which aids the validity of the murine model to assess the probe's tumor selectivity relative to lower levels of EGFR expression in healthy tissue including liver. Modest liver accumulation was observed (4.8 ± 1.8%ID/g at 2 h), which was due to physiological processing, not EGFR targeting, as the nonbinding control exhibited equivalent hepatic retention (4.9 ± 1.8%ID/g). This liver signal remains below the EGFR^{high} tumor signal (1.5 ± 0.4 tumor/liver). Nevertheless, efforts are underway to mutate surface hydrophobic amino acids to increase Gp2 hydrophilicity, which effectively reduced liver signal for engineered fibronectin domains.[29]

The relevance of noninvasive EGFR detection in the clinic has led to development of many imaging probes, including a variety of small protein scaffolds. The increased extravasation and tissue penetration of protein scaffolds compared to larger proteins allows for high contrast early imaging resulting in lower patient dose. Multiple successes have been realized for EGFR previously. The beneficial properties of Gp2 domains as evolvable protein scaffolds, such as small size, lack of cysteines, and high thermal stability, do not guarantee successful translation to an imaging agent. However, these properties provide benefits during evolution, conjugation, administration, and biodistribution that are useful for imaging agents or therapeutics toward many targets. Due to the variations between laboratories, strict quantitative comparisons between scaffolds do not prove superiority. Moreover, comparisons across scaffolds must take care to acknowledge the context-dependent properties, affinity, charge, hydrophilicity, of individual protein variants. Nevertheless, the current data demonstrate that the Gp2 domain is a promising PET imaging agent for EGFR with potential benefits versus other probes, and further optimization of the affinity and biophysical properties of Gp2-EGFR could lead to a clinically effective PET imaging agent. ^{64}Cu-Gp2-EGFR exhibits tumor accumulation (3.2 ± 0.5%ID/g at 0.75 h via PET; 7.0 ± 1.9%ID/g at 2 h via excised tissue) comparable to other small protein PET probes including fibronectin domains (3.4 ± 1.0 and 2.4 ± 1.0%ID/g at 1 h)[28] and affibodies (5.7 ± 0.6 and 9.7 ± 4.9%ID/g at 1 h)[30] as well as nanobodies for single-photon emission computed tomography (4.6 ± 0.4%ID/g at 1 h).[37] The dramatically lower uptake of ^{64}Cu-Gp2-EGFR in EGFR^{low} tumors and nonbinding control in EGFR^{high} tumors was similarly observed for the fibronectin domain. For affibody, neither EGFR^{low} tumors nor nontargeted affibody were evaluated as controls. Blocking did yield a reduction, albeit incomplete (47%), in EGFR^{high} tumor uptake. ^{64}Cu-Gp2-EGFR exhibits high tumor/blood ratio (14 ± 8 at 2 h) because of rapid clearance (3.2 ± 1.0 min half-time). Conversely, affibody provides limited tumor/blood differentiation (1.2 ± 1.1 and 1.0 ± 0.1 at 1 and 4 h) because of slower clearance (20−120 min half-time[30,59−62]) while fibronectin is intermediate (8.9 ± 4.7 and 6.4 ± 4.3 at 1 and

DOI: 10.1021/acs.molpharmaceut.6b00538
Mol. Pharmaceutics 2016, 13, 3747−3755

4 h[28]) with rapid clearance (2.1 ± 0.3 min half-time[28]). Tumor/muscle specificity is also strong for ^{64}Cu-Gp2-EGFR (11 ± 6 at 0.75 h via PET; 23 ± 6 at 2 h via excised tissue), comparable to affibody (16 ± 7 at 1 h, 18 ± 4 at 4 h, both via excised tissue) and higher than fibronectin (8.6 ± 3.0 at 1 h via PET; 10 ± 4 and 4.2 ± 1.3 at 1 and 4 h via excised tissue).

The main disadvantage of Gp2 as an imaging agent is the high kidney signal due to partial renal retention during clearance, which is observed for most small protein scaffolds.[43] Dosimetry calculations indicate 3.0 mGy/MBq renal dose, which is 3% of the maximum tolerated dose for a 185 MBq injection thereby rendering this a minor concern clinically for nonrenal tumors. Yet strategies exist to lower kidney signal. Modulation of charge has been shown to reduce renal uptake in fibronectin domains,[29] affibodies,[63] and knottins.[64] Preliminary data indicate an ability to modify charge on Gp2-EGFR while retaining activity. Additionally, alternative radiochemical conjugation has drastically reduced renal uptake of other small protein scaffolds.[62,65−70] Specifically, transchelation from the DOTA chelator[71] may account for some signal in the liver and kidney, and other chelators such as NOTA or PCTA have shown higher stability in vivo.[72] Notably, ^{64}Cu ($t_{1/2}$ = 12.7 h) was used in the current study to enable examination of distribution kinetics over short and long time periods, which is important for initial physiological characterization of this new protein scaffold. Yet, clinical use may benefit from a radioisotope with decay kinetics that align with the rapid distribution of the small Gp2 domain to reduce patient dose. Future studies with ^{18}F ($t_{1/2}$ = 110 min), ^{68}Ga ($t_{1/2}$ = 68 min), or ^{61}Cu ($t_{1/2}$ = 3.3 h) will be valuable for clinical translation. Evaluation on cells with intermediate EGFR expression will also be informative. It should be noted that, as with any synthetically engineered protein with nonhuman sequence components, immunogenicity of evolved molecules will need to be evaluated.

Overall, the performance of these initial Gp2 domains *in vivo* gives promise to the potential of Gp2-EGFR, and other targeted Gp2 domains, as molecular imaging agents.

■ ASSOCIATED CONTENT

Supporting Information

The Supporting Information is available free of charge on the ACS Publications website at DOI: 10.1021/acs.molpharmaceut.6b00538.

Mass spectrometry verification of DOTA conjugation, size exclusion chromatography results, murine EGFR affinity titration curve, EGFR receptor quantification (PDF)

■ AUTHOR INFORMATION

Corresponding Author

*E-mail: hackel@umn.edu. Phone: 612-624-7102.

Notes

The authors declare the following competing financial interest(s): M.A.K. and B.J.H. have a pending patent application related to Gp2 domain engineering and application.

■ ACKNOWLEDGMENTS

We are grateful to Joanne Johnson of the Center for Clinical Imaging Research for assistance with PET/CT imaging and Dr. Blake Jacobson from the Department of Medicine at the University of Minnesota for assistance with *ex vivo* tumor analysis. This work was funded by the National Institutes of Health (EB019518 to BJH), Komen for the Cure (SAC110039 to DY), National Cancer Institute Cancer Center Support Grant P30 077598, and the University of Minnesota.

■ ABBREVIATIONS

EGFR, epidermal growth factor; PET, positron emission tomography; DOTA, 1,4,7,10-tetraazacyclododecane-1,4,7,10-tetraacetic acid; CT, computed tomography; PBS, phosphate buffered saline; SDS-PAGE, sodium dodecyl sulfate−polyacrylamide gel electrophoresis

■ REFERENCES

(1) Hamburg, M. A.; Collins, F. S. The Path to Personalized Medicine. *N. Engl. J. Med.* **2010**, *363* (4), 301−304.

(2) Scott, A. M.; Wolchok, J. D.; Old, L. J. Antibody Therapy of Cancer. *Nat. Rev. Cancer* **2012**, *12* (4), 278−287.

(3) Kircher, M. F.; Hricak, H.; Larson, S. M. Molecular Imaging for Personalized Cancer Care. *Mol. Oncol.* **2012**, *6* (2), 182−195.

(4) Hynes, N. E.; MacDonald, G. ErbB Receptors and Signaling Pathways in Cancer. *Curr. Opin. Cell Biol.* **2009**, *21* (2), 177−184.

(5) Shinojima, N.; Tada, K.; Shiraishi, S.; Kamiryo, T.; Kochi, M.; Nakamura, H.; Makino, K.; Saya, H.; Hirano, H.; Kuratsu, J.-I.; Oka, K.; Ishimaru, Y.; Ushio, Y. Prognostic Value of Epidermal Growth Factor Receptor in Patients with Glioblastoma Multiforme. *Cancer Res.* **2003**, *63* (20), 6962−6970.

(6) Nieto, Y.; Nawaz, F.; Jones, R. B.; Shpall, E. J.; Nawaz, S. Prognostic Significance of Overexpression and Phosphorylation of Epidermal Growth Factor Receptor (EGFR) and the Presence of Truncated EGFRvIII in Locoregionally Advanced Breast Cancer. *J. Clin. Oncol.* **2007**, *25* (28), 4405−4413.

(7) Lugli, A.; Iezzi, G.; Hostettler, I.; Muraro, M. G.; Mele, V.; Tornillo, L.; Carafa, V.; Spagnoli, G.; Terracciano, L.; Zlobec, I. Prognostic Impact of the Expression of Putative Cancer Stem Cell Markers CD133, CD166, CD44s, EpCAM, and ALDH1 in Colorectal Cancer. *Br. J. Cancer* **2010**, *103* (3), 382−390.

(8) Galizia, G.; Lieto, E.; Orditura, M.; Castellano, P.; La Mura, A.; Imperatore, V.; Pinto, M.; Zamboli, A.; De Vita, F.; Ferraraccio, F. Epidermal Growth Factor Receptor (EGFR) Expression Is Associated with a Worse Prognosis in Gastric Cancer Patients Undergoing Curative Surgery. *World J. Surg.* **2007**, *31* (7), 1458−1468.

(9) Parra, H. S.; Cavina, R.; Latteri, F.; Zucali, P. A.; Campagnoli, E.; Morenghi, E.; Grimaldi, G. C.; Roncalli, M.; Santoro, A. Analysis of Epidermal Growth Factor Receptor Expression as a Predictive Factor for Response to Gefitinib ("Iressa", ZD1839) in Non-Small-Cell Lung Cancer. *Br. J. Cancer* **2004**, *91*, 208−212.

(10) Schlomm, T.; Kirstein, P.; Iwers, L.; Daniel, B.; Steuber, T.; Walz, J.; Chun, F. H. K.; Haese, A.; Kollermann, J.; Graefen, M.; Huland, H.; Sauter, G.; Simon, R.; Erbersdobler, A. Clinical Significance of Epidermal Growth Factor Receptor Protein Overexpression and Gene Copy Number Gains in Prostate Cancer. *Clin. Cancer Res.* **2007**, *13*, 6579−6584.

(11) Huang, C.-W.; Tsai, H.-L.; Chen, Y.-T.; Huang, C.-M.; Ma, C.-J.; Lu, C.-Y.; Kuo, C.-H.; Wu, D.-C.; Chai, C.-Y.; Wang, J.-Y. The Prognostic Values of EGFR Expression and KRAS Mutation in Patients with Synchronous or Metachronous Metastatic Colorectal Cancer. *BMC Cancer* **2013**, *13* (1), 599.

(12) Rokita, M.; Stec, R.; Bodnar, L.; Charkiewicz, R.; Korniluk, J.; Smoter, M.; Cichowicz, M.; Chyczewski, L.; Nikliński, J.; Kozłowski, W.; Szczylik, C. Overexpression of Epidermal Growth Factor Receptor as a Prognostic Factor in Colorectal Cancer on the Basis of the Allred Scoring System. *OncoTargets Ther.* **2013**, *6*, 967−976.

(13) Laurent-Puig, P.; Cayre, A.; Manceau, G.; Buc, E.; Bachet, J.-B.; Lecomte, T.; Rougier, P.; Lievre, A.; Landi, B.; Boige, V.; Ducreux, M.; Ychou, M.; Bibeau, F.; Bouché, O.; Reid, J.; Stone, S.; Penault-Llorca, F. Analysis of PTEN, BRAF, and EGFR Status in Determining Benefit from Cetuximab Therapy in Wild-Type KRAS Metastatic Colon Cancer. *J. Clin. Oncol.* **2009**, *27* (35), 5924−5930.

DOI: 10.1021/acs.molpharmaceut.6b00538
Mol. Pharmaceutics 2016, 13, 3747−3755

(14) Scartozzi, M.; Bearzi, I.; Mandolesi, A.; Pierantoni, C.; Loupakis, F.; Zaniboni, A.; Negri, F.; Quadri, A.; Zorzi, F.; Galizia, E.; Berardi, R.; Biscotti, T.; Labianca, R.; Masi, G.; Falcone, A.; Cascinu, S. Epidermal Growth Factor Receptor (EGFR) Gene Copy Number (GCN) Correlates with Clinical Activity of Irinotecan-Cetuximab in K-RAS Wild-Type Colorectal Cancer: A Fluorescence in Situ (FISH) and Chromogenic in Situ Hybridization (CISH) Analysis. *BMC Cancer* **2009**, *9*, 303.

(15) Moroni, M.; Veronese, S.; Benvenuti, S.; Marrapese, G.; Sartore-Bianchi, A.; Di Nicolantonio, F.; Gambacorta, M.; Siena, S.; Bardelli, A. Gene Copy Number for Epidermal Growth Factor Receptor (EGFR) and Clinical Response to antiEGFR Treatment in Colorectal Cancer: A Cohort Study. *Lancet Oncol.* **2005**, *6* (5), 279−286.

(16) Lee, H. J.; Seo, A. N.; Kim, E. J.; Jang, M. H.; Kim, Y. J.; Kim, J. H.; Kim, S.-W.; Ryu, H. S.; Park, I. A.; Im, S.-A.; Gong, G.; Jung, K. H.; Kim, H. J.; Park, S. Y. Prognostic and Predictive Values of EGFR Overexpression and EGFR Copy Number Alteration in HER2-Positive Breast Cancer. *Br. J. Cancer* **2015**, *112* (1), 103−111.

(17) Scartozzi, M.; Bearzi, I.; Berardi, R.; Mandolesi, A.; Fabris, G.; Cascinu, S. Epidermal Growth Factor Receptor (EGFR) Status in Primary Colorectal Tumors Does Not Correlate with EGFR Expression in Related Metastatic Sites: Implications for Treatment with EGFR-Targeted Monoclonal Antibodies. *J. Clin. Oncol.* **2004**, *22* (23), 4772−4778.

(18) Yarom, N.; Marginean, C.; Moyana, T.; Gorn-Hondermann, I.; Birnboim, H. C.; Marginean, H.; Auer, R. C.; Vickers, M.; Asmis, T. R.; Maroun, J.; Jonker, D. EGFR Expression Variance in Paired Colorectal Cancer Primary and Metastatic Tumors. *Cancer Biol. Ther.* **2010**, *10* (5), 416−421.

(19) Bozzetti, C.; Tiseo, M.; Lagrasta, C.; Nizzoli, R.; Guazzi, A.; Leonardi, F.; Gasparro, D.; Spiritelli, E.; Rusca, M.; Carbognani, P.; Majori, M.; Franciosi, V.; Rindi, G.; Ardizzoni, A. Comparison between Epidermal Growth Factor Receptor (EGFR) Gene Expression in Primary Non-Small Cell Lung Cancer (NSCLC) and in Fine-Needle Aspirates from Distant Metastatic Sites. *J. Thorac. Oncol.* **2008**, *3* (1), 18−22.

(20) Linden, H. M.; Stekhova, S. A.; Link, J. M.; Gralow, J. R.; Livingston, R. B.; Ellis, G. K.; Petra, P. H.; Peterson, L. M.; Schubert, E. K.; Dunnwald, L. K.; Krohn, K. A.; Mankoff, D. A. Quantitative Fluoroestradiol Positron Emission Tomography Imaging Predicts Response to Endocrine Treatment in Breast Cancer. *J. Clin. Oncol.* **2006**, *24* (18), 2793−2799.

(21) Peterson, L. M.; Kurland, B. F.; Schubert, E. K.; Link, J. M.; Gadi, V. K.; Specht, J. M.; Eary, J. F.; Porter, P.; Shankar, L. K.; Mankoff, D. A.; Linden, H. M. A Phase 2 Study of 16α-[18F]-Fluoro-17β-Estradiol Positron Emission Tomography (FES-PET) as a Marker of Hormone Sensitivity in Metastatic Breast Cancer (MBC). *Mol. Imaging Biol.* **2014**, *16* (3), 431−440.

(22) Cai, W.; Chen, K.; He, L.; Cao, Q.; Koong, A.; Chen, X. Quantitative PET of EGFR Expression in Xenograft-Bearing Mice Using 64Cu-Labeled Cetuximab, a Chimeric Anti-EGFR Monoclonal Antibody. *Eur. J. Nucl. Med. Mol. Imaging* **2007**, *34* (6), 850−858.

(23) Niu, G.; Li, Z.; Xie, J.; Le, Q.-T.; Chen, X. PET of EGFR Antibody Distribution in Head and Neck Squamous Cell Carcinoma Models. *J. Nucl. Med.* **2009**, *50* (7), 1116−1123.

(24) Niu, G.; Sun, X.; Cao, Q.; Courter, D.; Koong, A.; Le, Q.-T.; Gambhir, S. S.; Chen, X. Cetuximab-Based Immunotherapy and Radioimmunotherapy of Head and Neck Squamous Cell Carcinoma. *Clin. Cancer Res.* **2010**, *16* (7), 2095−2105.

(25) Ping Li, W.; Meyer, L. A.; Capretto, D. A.; Sherman, C. D.; Anderson, C. J. Receptor-Binding, Biodistribution, and Metabolism Studies of 64Cu-DOTA-Cetuximab, a PET-Imaging Agent for Epidermal Growth-Factor Receptor-Positive Tumors. *Cancer Biother.Radiopharm.* **2008**, *23* (2), 158−171.

(26) Menke-van der Houven van Oordt, C. W.; Gootjes, E. C.; Huisman, M. C.; Vugts, D. J.; Roth, C.; Luik, A. M.; Mulder, E. R.; Schuit, R. C.; Boellaard, R.; Hoekstra, O. S.; van Dongen, G. A. M. S.; Verheul, H. M. W. Zr-Cetuximab PET Imaging in Patients with Advanced Colorectal Cancer. *Oncotarget* **2015**, *6* (30), 4672.

(27) Bhattacharyya, S.; Kurdziel, K.; Wei, L.; Riffle, L.; Kaur, G.; Hill, G. C.; Jacobs, P. M.; Tatum, J. L.; Doroshow, J. H.; Kalen, J. D. Zirconium-89 Labeled Panitumumab: A Potential Immuno-PET Probe for HER1-Expressing Carcinomas. *Nucl. Med. Biol.* **2013**, *40* (4), 451−457.

(28) Hackel, B. J.; Kimura, R. H.; Gambhir, S. S. Use of 64Cu-Labeled Fibronectin Domain with EGFR-Overexpressing Tumor Xenograft: Molecular Imaging. *Radiology* **2012**, *263* (1), 179−188.

(29) Hackel, B. J.; Sathirachinda, A.; Gambhir, S. S. Designed Hydrophilic and Charge Mutations of the Fibronectin Domain: Towards Tailored Protein Biodistribution. *Protein Eng., Des. Sel.* **2012**, *25* (10), 639−647.

(30) Miao, Z.; Ren, G.; Hongguang, L.; Jiang, L.; Cheng, Z. Small-Animal PET Imaging of Human Epidermal Growth Factor Receptor Positive Tumor with a 64Cu Labeled Affibody Protein. *Bioconjugate Chem.* **2010**, *21* (5), 947−954.

(31) Miao, Z.; Ren, G.; Liu, H.; Qi, S.; Wu, S.; Cheng, Z. PET of EGFR Expression with an 18F-Labeled Affibody Molecule. *J. Nucl. Med.* **2012**, *53* (7), 1110−1118.

(32) Nordberg, E.; Orlova, A.; Friedman, M.; Tolmachev, V.; Ståhl, S.; Nilsson, F. Y.; Glimelius, B.; Carlsson, J. In Vivo and in Vitro Uptake of 111In, Delivered with the Affibody Molecule (ZEGFR:955)2, in EGFR Expressing Tumour Cells. *Oncol. Rep.* **2008**, *19* (4), 853−857.

(33) Tolmachev, V.; Rosik, D.; Wållberg, H.; Sjöberg, A.; Sandström, M.; Hansson, M.; Wennborg, A.; Orlova, A. Imaging of EGFR Expression in Murine Xenografts Using Site-Specifically Labelled Anti-EGFR 111In-DOTA-Z EGFR:2377 Affibody Molecule: Aspect of the Injected Tracer Amount. *Eur. J. Nucl. Med. Mol. Imaging* **2010**, *37* (3), 613−622.

(34) Su, X.; Cheng, K.; Jeon, J.; Shen, B.; Venturin, G. T.; Hu, X.; Rao, J.; Chin, F. T.; Wu, H.; Cheng, Z. Comparison of Two Site-Specifically 18F-Labeled Affibodies for PET Imaging of EGFR Positive Tumors. *Mol. Pharmaceutics* **2014**, *11* (11), 3947−3956.

(35) Huang, L.; Gainkam, L. O. T.; Caveliers, V.; Vanhove, C.; Keyaerts, M.; De Baetselier, P.; Bossuyt, A.; Revets, H.; Lahoutte, T. SPECT Imaging with 99mTc-Labeled EGFR-Specific Nanobody for in Vivo Monitoring of EGFR Expression. *Mol. Imaging Biol.* **2008**, *10* (3), 167−175.

(36) Gainkam, L. O. T.; Keyaerts, M.; Caveliers, V.; Devoogdt, N.; Vanhove, C.; Van Grunsven, L.; Muyldermans, S.; Lahoutte, T. Correlation between Epidermal Growth Factor Receptor-Specific Nanobody Uptake and Tumor Burden: A Tool for Noninvasive Monitoring of Tumor Response to Therapy. *Mol. Imaging Biol.* **2011**, *13* (5), 940−948.

(37) Gainkam, L. O. T.; Huang, L.; Caveliers, V.; Keyaerts, M.; Hernot, S.; Vaneycken, I.; Vanhove, C.; Revets, H.; De Baetselier, P.; Lahoutte, T. Comparison of the Biodistribution and Tumor Targeting of Two 99mTc-Labeled Anti-EGFR Nanobodies in Mice, Using Pinhole SPECT/micro-CT. *J. Nucl. Med.* **2008**, *49* (5), 788−795.

(38) Chakravarty, R.; Goel, S.; Valdovinos, H. F.; Hernandez, R.; Hong, H.; Nickles, R. J.; Cai, W. Matching the Decay Half-Life with the Biological Half-Life: ImmunoPET Imaging with44Sc-Labeled Cetuximab Fab Fragment. *Bioconjugate Chem.* **2014**, *25* (12), 2197−2204.

(39) Schmidt, M. M.; Wittrup, K. D. A Modeling Analysis of the Effects of Molecular Size and Binding Affinity on Tumor Targeting. *Mol. Cancer Ther.* **2009**, *8* (10), 2861−2871.

(40) Zahnd, C.; Kawe, M.; Stumpp, M. T.; de Pasquale, C.; Tamaskovic, R.; Nagy-Davidescu, G.; Dreier, B.; Schibli, R.; Binz, H. K.; Waibel, R.; Plückthun, A. Efficient Tumor Targeting with High-Affinity Designed Ankyrin Repeat Proteins: Effects of Affinity and Molecular Size. *Cancer Res.* **2010**, *70* (4), 1595−1605.

(41) Yuan, F.; Dellian, M.; Fukumura, D.; Leunig, M.; Berk, D. A.; Torchilin, V. P.; Jain, R. K. Vascular Permeability in a Human Tumor Xenograft: Molecular Size Dependence and Cutoff Size. *Cancer Res.* **1995**, *55* (17), 3752−3756.

DOI: 10.1021/acs.molpharmaceut.6b00538
Mol. Pharmaceutics 2016, 13, 3747−3755

(42) Thurber, G. M.; Wittrup, K. D. Quantitative Spatiotemporal Analysis of Antibody Fragment Diffusion and Endocytic Consumption in Tumor Spheroids. *Cancer Res.* **2008**, *68* (9), 3334−3341.
(43) Stern, L. A.; Case, B. A.; Hackel, B. J. Alternative Non-Antibody Protein Scaffolds for Molecular Imaging of Cancer. *Curr. Opin. Chem. Eng.* **2013**, *2* (4), 425−432.
(44) Memon, A. A.; Jakobsen, S.; Dagnaes-Hansen, F.; Sorensen, B. S.; Keiding, S.; Nexo, E. Positron Emission Tomography (PET) Imaging with [11C]-Labeled Erlotinib: A Micro-PET Study on Mice with Lung Tumor Xenografts. *Cancer Res.* **2009**, *69* (3), 873−878.
(45) Zhang, M. R.; Kumata, K.; Hatori, A.; Takai, N.; Toyohara, J.; Yamasaki, T.; Yanamoto, K.; Yui, J.; Kawamura, K.; Koike, S.; Ando, K.; Suzuki, K. [11C]Gefitinib ([11C]Iressa): Radiosynthesis, In Vitro Uptake, and In Vivo Imaging of Intact Murine Fibrosarcoma. *Mol. Imaging Biol.* **2010**, *12* (2), 181−191.
(46) Wang, H.; Yu, J.; Yang, G.; Song, X.; Sun, X.; Zhao, S.; Mu, D. Assessment of 11C-Labeled-4-N-(3-Bromoanilino)-6,7-Dimethoxyquinazoline as a Positron Emission Tomography Agent to Monitor Epidermal Growth Factor Receptor Expression. *Cancer Sci.* **2007**, *98* (9), 1413−1416.
(47) Dai, D.; Li, X.-F.; Wang, J.; Liu, J.-J.; Zhu, Y.-J.; Zhang, Y.; Wang, Q.; Xu, W.-G. Predictive Efficacy of ^{11} C-PD153035 PET Imaging for EGFR-Tyrosine Kinase Inhibitor Sensitivity in Non-Small Cell Lung Cancer Patients. *Int. J. Cancer* **2016**, *138* (4), 1003−1012.
(48) Bahce, I.; Smit, E. F.; Lubberink, M.; Van Der Veldt, A. A. M.; Yaqub, M.; Windhorst, A. D.; Schuit, R. C.; Thunnissen, E.; Heideman, D. A. M.; Postmus, P. E.; Lammertsma, A. A.; Hendrikse, N. H. Development of [11C]erlotinib Positron Emission Tomography for in Vivo Evaluation of EGF Receptor Mutational Status. *Clin. Cancer Res.* **2013**, *19* (1), 183−193.
(49) Slobbe, P.; Windhorst, A. D.; Walsum, M. S.; Schuit, R. C.; Smit, E. F.; Niessen, H. G.; Solca, F.; Stehle, G.; van Dongen, G. A. M. S.; Poot, A. J. Development of [18F]afatinib as New TKI-PET Tracer for EGFR Positive Tumors. *Nucl. Med. Biol.* **2014**, *41* (9), 749−757.
(50) Kareem, H.; Sandström, K.; Elia, R.; Gedda, L.; Anniko, M.; Lundqvist, H.; Nestor, M. Blocking EGFR in the Liver Improves the Tumor-to-Liver Uptake Ratio of Radiolabeled EGF. *Tumor Biol.* **2010**, *31* (2), 79−87.
(51) Kruziki, M. A.; Bhatnagar, S.; Woldring, D. R.; Duong, V. T.; Hackel, B. J. A 45-Amino-Acid Scaffold Mined from the PDB for High-Affinity Ligand Engineering. *Chem. Biol.* **2015**, *22* (7), 946−956.
(52) Chambers, A. F. MDA-MB-435 and M14 Cell Lines: Identical but Not M14 Melanoma? *Cancer Res.* **2009**, *69* (13), 5292−5293.
(53) Koide, A.; Bailey, C. W.; Huang, X.; Koide, S. The Fibronectin Type III Domain as a Scaffold for Novel Binding Proteins. *J. Mol. Biol.* **1998**, *284* (4), 1141−1151.
(54) Tamaskovic, R.; Simon, M.; Stefan, N.; Schwill, M.; Plückthun, A. Designed Ankyrin Repeat Proteins (DARPins) from Research to Therapy. *Methods Enzymol.* **2012**, *503*, 101−134.
(55) Moore, S. J.; Leung, C. L.; Cochran, J. R. Knottins: Disulfide-Bonded Therapeutic and Diagnostic Peptides. *Drug Discovery Today: Technol.* **2012**, *9* (1), e3−e11.
(56) Heinis, C.; Rutherford, T.; Freund, S.; Winter, G. Phage-Encoded Combinatorial Chemical Libraries Based on Bicyclic Peptides. *Nat. Chem. Biol.* **2009**, *5* (7), 502−507.
(57) Löfblom, J.; Feldwisch, J.; Tolmachev, V.; Carlsson, J.; Ståhl, S.; Frejd, F. Y. Affibody Molecules: Engineered Proteins for Therapeutic, Diagnostic and Biotechnological Applications. *FEBS Lett.* **2010**, *584* (12), 2670−2680.
(58) Hackel, B. J. Alternative Protein Scaffolds for Molecular Imaging and Therapy. In *Engineering in Translational Medicine*; Cai, W., Ed.; Springer: London, 2013; pp 343−364.
(59) Ahlgren, S.; Orlova, A.; Wallberg, H.; Hansson, M.; Sandstrom, M.; Lewsley, R.; Wennborg, A.; Abrahmsen, L.; Tolmachev, V.; Feldwisch, J. Targeting of HER2-Expressing Tumors Using 111In-ABY-025, a Second-Generation Affibody Molecule with a Fundamentally Reengineered Scaffold. *J. Nucl. Med.* **2010**, *51* (7), 1131−1138.
(60) Ahlgren, S.; Wallberg, H.; Tran, T. A.; Widstrom, C.; Hjertman, M.; Abrahmsen, L.; Berndorff, D.; Dinkelborg, L. M.; Cyr, J. E.; Feldwisch, J.; Orlova, A.; Tolmachev, V. Targeting of HER2-Expressing Tumors with a Site-Specifically 99mTc-Labeled Recombinant Affibody Molecule, ZHER2:2395, with C-Terminally Engineered Cysteine. *J. Nucl. Med.* **2009**, *50* (5), 781−789.
(61) Kramer-Marek, G.; Kiesewetter, D. O.; Martiniova, L.; Jagoda, E.; Lee, S. B.; Capala, J. [18F]FBEM-ZHER2:342−Affibody Molecule—a New Molecular Tracer for in Vivo Monitoring of HER2 Expression by Positron Emission Tomography - Springer. *Eur. J. Nucl. Med. Mol. Imaging* **2008**, *35* (5), 1008−1018.
(62) Cheng, Z.; De Jesus, O. P.; Namavari, M.; De, A.; Levi, J.; Webster, J. M.; Zhang, R.; Lee, B.; Syud, F. A.; Gambhir, S. S. Small-Animal PET Imaging of Human Epidermal Growth Factor Receptor Type 2 Expression with Site-Specific 18F-Labeled Protein Scaffold Molecules. *J. Nucl. Med.* **2008**, *49* (5), 804−813.
(63) Tran, T.; Engfeldt, T.; Orlova, A.; Sandström, M.; Feldwisch, J.; Abrahmsén, L.; Wennborg, A.; Tolmachev, V.; Karlström, A. E. 99m Tc-maEEE-Z HER2:342, an Affibody Molecule-Based Tracer for the Detection of HER2 Expression in Malignant Tumors. *Bioconjugate Chem.* **2007**, *2*, 1956−1964.
(64) Kimura, R. H.; Teed, R.; Hackel, B. J.; Pysz, M. A.; Chuang, C. Z.; Sathirachinda, A.; Willmann, J. K.; Gambhir, S. S. Pharmacokinetically Stabilized Cystine Knot Peptides That Bind Alpha-v-Beta-6 Integrin with Single-Digit Nanomolar Affinities for Detection of Pancreatic Cancer. *Clin. Cancer Res.* **2012**, *18* (3), 839−849.
(65) Cheng, Z.; De Jesus, O. P.; Kramer, D. J.; De, A.; Webster, J. M.; Gheysens, O.; Levi, J.; Namavari, M.; Wang, S.; Park, J. M.; Zhang, R.; Liu, H.; Lee, B.; Syud, F. A.; Gambhir, S. S. 64Cu-Labeled Affibody Molecules for Imaging of HER2 Expressing Tumors. *Mol. Imaging Biol.* **2010**, *12* (3), 316−324.
(66) Ahlgren, S.; Orlova, A.; Rosik, D.; Sandström, M.; Sjöberg, A.; Baastrup, B.; Widmark, O.; Fant, G.; Feldwisch, J.; Tolmachev, V. Evaluation of Maleimide Derivative of DOTA for Site-Specific Labeling of Recombinant Affibody Molecules. *Bioconjugate Chem.* **2008**, *19* (1), 235−243.
(67) Tolmachev, V.; Friedman, M.; Sandström, M.; Eriksson, T. L. J.; Rosik, D.; Hodik, M.; Ståhl, S.; Frejd, F. Y.; Orlova, A. Affibody Molecules for Epidermal Growth Factor Receptor Targeting in Vivo: Aspects of Dimerization and Labeling Chemistry. *J. Nucl. Med.* **2009**, *50* (2), 274−283.
(68) Tolmachev, V.; Nilsson, F. Y.; Widström, C.; Andersson, K.; Rosik, D.; Gedda, L.; Wennborg, A.; Orlova, A. 111In-Benzyl-DTPA-ZHER2:342, an Affibody-Based Conjugate for in Vivo Imaging of HER2 Expression in Malignant Tumors. *J. Nucl. Med.* **2006**, *47* (5), 846−853.
(69) Orlova, A.; Wållberg, H.; Stone-Elander, S.; Tolmachev, V. On the Selection of a Tracer for PET Imaging of HER2-Expressing Tumors: Direct Comparison of a 124I-Labeled Affibody Molecule and Trastuzumab in a Murine Xenograft Model. *J. Nucl. Med.* **2009**, *50* (3), 417−425.
(70) Kramer-Marek, G.; Kiesewetter, D. O.; Capala, J. Changes in HER2 Expression in Breast Cancer Xenografts after Therapy Can Be Quantified Using PET and (18)F-Labeled Affibody Molecules. *J. Nucl. Med.* **2009**, *50* (7), 1131−1139.
(71) Boswell, C. A.; Sun, X.; Niu, W.; Weisman, G. R.; Wong, E. H.; Rheingold, A. L.; Anderson, C. J. Comparative in Vivo Stability of Copper-64-Labeled Cross-Bridged and Conventional Tetraazamacrocyclic Complexes. *J. Med. Chem.* **2004**, *47* (6), 1465−1474.
(72) Ait-Mohand, S.; Fournier, P.; Dumulon-Perreault, V.; Kiefer, G. E.; Jurek, P.; Ferreira, C. L.; Benard, F.; Guerin, B. Evaluation of 64Cu-Labeled Bifunctional Chelate-Bombesin Conjugates. *Bioconjugate Chem.* **2011**, *22* (8), 1729−1735.

DOI: 10.1021/acs.molpharmaceut.6b00538
Mol. Pharmaceutics 2016, 13, 3747−3755